ISSN 1068-3372, Journal of Contemporary Physics (Armenian Academy of Sciences), 2023, Vol. 58, No. 1, pp. 14–23. © Pleiades Publishing, Ltd., 2023.
Russian Text © The Author(s), 2023, published in Izvestiya Natsional'noi Akademii Nauk Armenii, Fizika, 2023, Vol. 58, No. 1, pp. 22–35.

Electron Beam Loss Monitor of Areal Accelerator Based on Pin-Photodiodes

S. G. Arutyunyan[a, b], A. V. Margaryan[b], E. G. Lazareva[b, *], M. Chung[c], G. V. Mirzoyan[b], N. S. Mesropyan[b], V. G. Khachatryan[a], and A. D. Davtyan[a]

[a] *“Candle” Synchrotron Research Institute, Yerevan, Armenia*
[b] *Alikhanyan National Science Laboratory, Yerevan, Armenia*
[c] *Ulsan National Institute of Science and Technology, Ulsan, South Korea*
**e-mail: ella.lazareva@yerphi.am*

Received September 29, 2022; revised October 10, 2022; accepted November 16, 2022

Abstract—A prototype PIN-photodiode-based electron system for flux measurement of the AREAL accelerator electron beam (energy up to 5 MeV) was developed and tested. The system can be eventually used to measure beam losses from the vacuum chamber of the SASE100 undulator, which is intended for the generation of radiation in the terahertz range and will be installed in the AREAL accelerator tract during its modernization. The method of using the PIN-photodiodes as a beam loss monitor is based on the effect of electron–hole pairs formation when ionizing particles pass through the photodiode barrier layer. Calculations of the interaction of electrons with the substance of the barrier layer are performed using the PCLab program. The experiments carried out on the accelerator electron beam showed that the developed system can effectively register the electron fluxes of both the main beam of the AREAL accelerator and its dark current.

Keywords: beam loss monitor, PIN-photodiode, AREAL accelerator

DOI: 10.1134/S1068337223010061

1. INTRODUCTION

The AREAL accelerator modernization program is based on increasing the electron beam energy up to 20/50 MeV and includes the development of a terahertz radiation source based on the SASE100 undulator, which is supposed to use the self-amplified spontaneous emission principle (SASE) [1]. The ALPHA station with such a radiation source will be one of the promising devices of the AREAL accelerator.

The SASE100 undulator with a magnetic system frequency of 27.3 mm and a segment length of 4.4922 m is designed to create an alternating magnetic field of 0.47 T in a gap of 12 mm in the vertical direction [2]. In further computations, the vacuum chamber of the undulator is modeled as a rectangular profile with external dimensions of 20×15 mm^2 and a thickness of ≈ 2 mm (the material is aluminum). The magnetic system of the undulator is assembled on permanent NdFeB magnets with a residual magnetic induction of ≈ 1.2 T at a coercive field of 1400–600 kA/m and temperatures up to 60°C. For such magnets, radiation damage caused by electron beam losses can become a big problem. Particularly dangerous are emergencies when beam losses are caused not by a weak flux of peripheral particles of the beam (regular losses), but by the deboarding of the entire beam on the chamber walls. To prevent such situations, it is necessary to develop and install a beam loss system taking into account the design features of the undulator. Figure 1 shows a general view of the undulator and a fragment of the vacuum chamber.

As can be seen from Fig.1b, because of the limitation of the vacuum chamber in the vertical direction by poles and permanent magnets, the space available for the introduction of sensors in the horizontal direction is small. This circumstance limits the choice of possible methods for diagnosing beam losses by practically two methods: using optical fibers [3] and compact PIN photodiodes [4–7].

2. OPTICAL FIBERS. PIN PHOTODIODES

In the case of optical fibers, the physical effects that determine the passage of particles/radiation through the fiber can be the radiation turbidity of the fiber, or (at low irradiation intensities and high ener-

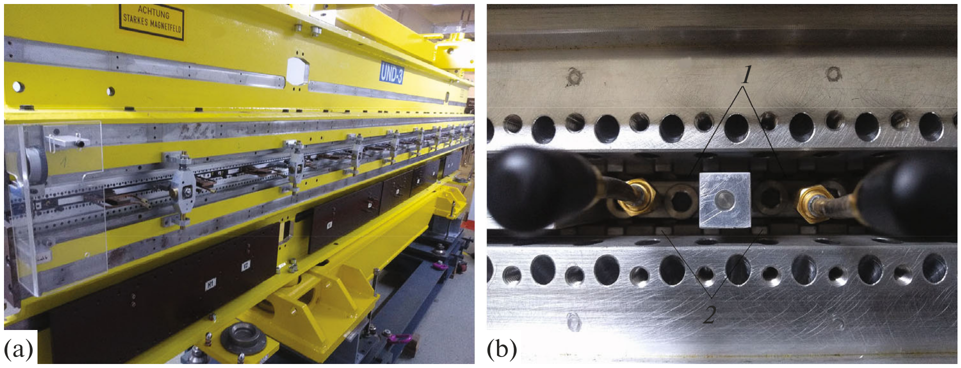

Fig. 1. (a) General view of the SASE100 undulator. (b) Fragment of the vacuum chamber and the magnetic system of the undulator: *1*—poles of the magnetic system, *2*—permanent magnets with horizontal polarization.

gies of the detected particles) the measurement of Cherenkov photons generated when particles pass through the fiber. In this case, the localization of the region of interaction of the beam with the fiber requires fast measurements of sufficiently small signals (a spatial resolution of about 20 cm requires measurements in the region of 1 ns [4]). In [3], systems for monitoring beam losses using optical fibers of kilometer lengths are discussed, while the spatial resolution reaches several meters.

The PIN photodiodes are widely used for detecting X- and γ-rays, as well as charged particles. The method is based on the effect of the formation of electron-hole pairs during the passage of particles through a substance. Generation of an electron-hole pair requires ≈3.6 eV of energy. In the presence of an electric field, the formed electrons drift toward the N region, while holes drift toward the P region. The PIN photodiodes differ from other types in that they contain a sufficiently thick (several hundred micrometers) blocking layer, on which a significant transfer of the energy of a passing particle to this layer occurs. The energy required to create an electron-hole pair in a semiconductor is approximately 10 times less than to create an electron/ion pair in a gas. In addition, the density of a semiconductor is about three orders of magnitude greater than that of a gas. Therefore, an ionizing particle creates a much larger signal per path length in a semiconductor than in a volume of gas. Accordingly, PIN photodiodes are often referred to as solid-state ionization chambers [4, 8, 9]. A significant advantage of conventional ionization chambers is that PIN photodiodes require low-voltage power.

2.1. Registration of Photons, Charged Particles, and Neutrons

The PIN photodiodes are widely used for detecting X-ray and γ-radiation. HAMAMATSU has developed a particular class of X-ray photodiodes (see [10]). As advantages, the high detection efficiency, wide dynamic range, good radiation resistance, and low cost of silicon PIN photodiodes are noted in [11]. The PIN photodiode systems are used as detectors for the visualization of radiation doses in radiotherapy [12]. In [13], when developing detection systems for radiological equipment, the RD100A PIN photodiodes were used as a more affordable alternative to traditional ionization chambers in this area.

The using PIN photodiodes to detect losses in a charged particle beam was first discussed in 1987 (see [5]). In [14], an array of PIN photodiodes was considered for detecting charged particles during beam collisions in an accelerator SSC. In [15] a procedure was developed for calibrating PIN photodiodes with a silicon barrier layer to measure α-radiation from sources based on the isotopes 239Pu (Plutonium), 241Am (Americium), and 244Cm (Curium). Based on the most commonly used BPW34F PIN photodiodes, a system for detecting proton fluxes equivalent to large neutron fluences was developed [16]. A matrix of 7 × 7 photodiodes was assembled with distances between diodes of 3.8 mm. The 800 MeV protons from the Los Alamos Neutron Science Center accelerator (LANSCE) were used. To detect the muon flux in the T2K experiment (Tokai-to-Kamioka, the neutrino oscillation experiment), an array of 49 PIN photodiodes was used [17]. The HAMAMATSU S3590–08 PIN photodiodes with an active area of 10 × 10 mm^2 and a barrier layer thickness of 300 μm have been used. The photodiode system was previously tested on a 100 MeV electron beam at Kyoto University (number of electrons 10^7–10^9 electrons/pulse with the pulse repetition rate 15 Hz. In [18], PIN photodiodes were used as energy detectors for fragments of nuclear decay reactions.

Note that there are proposals to use PIN photodiodes for neutron detection with discrimination of gamma radiation. Both the direct capture of neutrons by photodiodes and the more preferable option of using plastic scintillators that convert fast neutrons into protons are discussed [19]. Protons in the energy range of 3–12 MeV are trapped in the silicon layer of the PIN photodiode generating a photocurrent. The method has shown its operability for the neutron source AmBe.

2.2. Isolation of Charged Particles Against the Background of Radiation. Choice of Beam Monitoring Method

In [4, 5, 7], to suppress the background of synchrotron radiation, the readout by the coincidence of the readings of two diodes located opposite each other was included. Such a beam loss monitoring system was installed in 1993 at the HERAP accelerator and was a useful diagnostic tool, including an important part of the superconducting magnet protection system. A second beam loss monitoring system was installed in 1994 at HERAe to study severe beam current limitation characterized by a very short electron beam lifetime (a total of 214 PIN photodiodes were installed around the entire ring). As a result, the accumulated beam current and its lifetime have been increased [5].

The choice between the above two methods for monitoring beam losses in this work was made in favor of PIN photodiodes because our group has gained some experience in using such photodiodes to measure the profiles of thin laser beams [7, 8, 20–22]. The PIN photodiodes were used in these studies to measure the fluxes of photons reflected from a vibrating string, where the string served as a miniature scanner. Another useful quality of photodiodes was used here, their operation speed. More than a hundred measurements were made during the half-cycle of the string vibration, which makes it possible to profile the cross-section of a focused laser beam with micrometric resolution. It is also planned to develop a system for measuring beam losses in the SASE100 undulator using the optical fiber method.

3. EVALUATION OF THE SENSITIVITY OF PIN PHOTODIODES

The number of electron-hole pairs during the passage of an ionizing particle through the barrier layer of a PIN photodiode depends on the type of charged particle, its energy, and the properties of the material of the barrier layer. The most common PIN photodiodes with a quartz blocking layer. The ratios between the scattering cross sections of competing processes, such as ionization losses, bremsstrahlung, Møller, and Bhabha scattering, and annihilation processes determine the dependence of particle losses on its type and energy [22]. High-energy electrons interact with matter mainly through bremsstrahlung, while high-energy photons interact through the formation of electron-positron pairs [23, 24].

The processes of interaction of electrons with matter were computed using the PCLab program developed at the Tomsk Polytechnic University, which includes all the main channels of electron/radiation interaction [9, 10, 25, 26]. Basic computations are normalized to one incoming electron.

The AREAL electron beam parameters are as follows: electron energy 20 MeV, pulse repetition rate 20 Hz, pulse charge 250 pC, average current 5 nA, beam cross section 0.25 cm^2, and average beam flux 1.25×1011 n_e/s/cm^2.

Figure 2 represents the trajectories of scattered/generated particles (computation results for several values of the angle of electron entry, the angles are counted from the normal to the barrier surface).

Table 1 shows the fluxes of secondary particles during the passage of one electron with an energy of 20 MeV through a 2 mm aluminum wall at different angles of incidence relative to the normal.

Table 1 uses the following designations: θ is the angle of electron entry, *d_Al* = 2 mm barrier thickness, *d_Al*_eff = *d_Al*/cos θ is the effective barrier thickness, *e_Nf* is the number of electrons at the output, *e_Ef* is the average electron energy at the output, *p_Ef* is the number of positrons at the output, *ph_Nf* is the number of photons at the output, *ph_Ef* is the average photon energy at the output.

As can be seen from Table 1, there are practically no positrons at the exit from the barrier, and electrons and photons are mainly observed with increasing average energy with an increase in the effective path thickness. The outgoing electrons and positrons mainly move in the direction of the incoming electron, and in further estimates, this fact will be taken into account.

The response of a PIN photodiode is estimated in the same way as in [4, 5], namely, by using the concept of the minimum ionizing particle (MIP), which loses 2 MeV for ionization per centimeter of the path regardless of its energy and type. The following parameters were adopted: the barrier layer *d_Si* = 100 μm, and reverse bias voltage 24 V. The energy required to create an electron-hole pair in silicon is ≈3.6 eV. The energy released by MIP in silicon is ≈3.7 MeV/cm (in [4], the loss of MIP for any material is taken in the

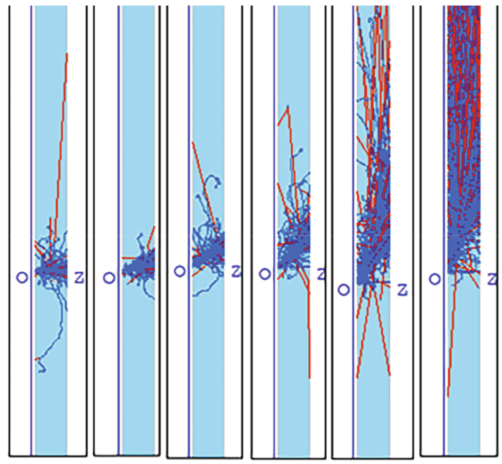

Fig. 2. Simulation of the passage of an electron through an aluminum layer 2 mm thick at different angles of incidence relative to the normal: 0, 15, 30, 45, 60, and 75°. The trajectories of secondary particles are depicted: electrons and photons.

range of 1–2 MeV/(g/cm^2), *Si* density is 2.33 g/cm^3). It is assumed that the surface of the photodiode is parallel to the surface of the vacuum chamber.

Table 2 gives estimates of the number of electron-hole pairs in the blocking layer of a PIN photodiode with a thickness of 100 μm from one electron, and the following designations are used: *d_Si*_eff = *d_Si*/cos θ is the effective thickness of the photodiode layer for particles incident at an angle; *e*_loss is the energy loss of electrons incident on the silicon barrier layer of the photodiode; *e_e*-holes is the number of electron holes generated by electrons; *p*_loss is the energy loss of positrons incident on the barrier layer; *p_e*-holes is the number of electron holes generated by positrons; *ph*_loss is the energy loss of photons incident on the barrier layer; *ph_e*-holes is the number of electron holes generated by photons; *F_e*-holes is the total number of generated electron holes.

Table 1. Integral characteristics of secondary particles/photons at the exit behind an aluminum barrier during the passage of one electron for different angles of incidence

θ	*d_Al*_eff, cm	*e_Nf*	*e_Ef*, MeV	*p_Nf*	*p_Ef*, MeV	*ph_Nf*	*ph_Ef*, MeV
0	0.2	1.05	18.8	5.10×10^{-5}	2.33×10^{-4}	0.177	0.33
15	0.207	1.05	18.8	6.00×10^{-5}	2.02×10^{-4}	0.182	0.34
30	0.231	1.06	18.6	6.90×10^{-5}	2.82×10^{-4}	0.201	0.375
45	0.283	1.07	18.3	8.50×10^{-5}	3.62×10^{-4}	0.245	0.463
60	0.4	1.08	17.5	1.83×10^{-4}	6.78×10^{-4}	0.347	0.653
75	0.773	0.994	13.1	6.12×10^{-4}	2.16×10^{-3}	0.591	1.06

Table 2. Computations of electron-hole pairs in the blocking layer of a PIN photodiode

θ	*d_Si*_eff, cm	*e*_loss, MeV	*e_e*-holes	*p*_loss, MeV	*p_e*-holes	*ph*_loss, MeV	*ph_e*-holes	*F_e*-holes
0	1.00×10^{-2}	3.89×10^{-2}	1.11×10^{4}	1.89×10^{-6}	0.539	6.53×10^{-3}	1.87×10^{3}	1.30×10^{4}
15	1.04×10^{-2}	4.04×10^{-2}	1.15×10^{4}	2.30×10^{-6}	0.657	6.97×10^{-3}	1.99×10^{3}	1.35×10^{4}
30	1.15×10^{-2}	4.52×10^{-2}	1.29×10^{4}	2.95×10^{-6}	0.842	8.61×10^{-3}	2.46×10^{3}	1.54×10^{4}
45	1.41×10^{-2}	5.57×10^{-2}	1.59×10^{4}	4.45×10^{-6}	1.27	1.28×10^{-2}	3.67×10^{3}	1.96×10^{4}
60	2.00×10^{-2}	8.00×10^{-2}	2.29×10^{4}	1.35×10^{-5}	3.87	2.57×10^{-2}	7.33×10^{3}	3.02×10^{4}
75	3.86×10^{-2}	1.42×10^{-1}	4.06×10^{4}	8.75×10^{-5}	25	8.44×10^{-2}	2.41×10^{4}	6.48×10^{4}

Table 3. Computation of the resolution current density in the photodiode region

S_eff, cm^2	N_e_e/s, cm^2	F_e, n_e/s	P_e, e-hole/s	I_detect, A/cm^2
6.60×10^{-2}	7.29×10^5	4.81×10^4	6.25×10^8	1.17×10^{-13}
6.38×10^{-2}	7.25×10^5	4.62×10^4	6.25×10^4	1.16×10^{-13}
5.72×10^{-2}	7.11×10^5	4.07×10^4	6.25×10^4	1.14×10^{-13}
4.67×10^{-2}	6.83×10^5	3.19×10^4	6.25×10^4	1.09×10^{-13}
3.30×10^{-2}	6.27×10^5	2.07×10^4	6.25×10^4	1.00×10^{-13}
1.71×10^{-2}	5.65×10^5	9.65×10^4	6.25×10^4	9.04×10^{-14}

Table 3 shows computations of the density of resolution current through the photodiode. As the resolution parameter, we chose the condition that the signal from electron-hole pairs is compared with the dark current of the photodiode at approximately 0.1 nA (the characteristic of Hamamatsu S1223 PIN photodiodes).

In Table 3, the following designations are used: S_eff = S_photodiode is the effective area of the photodiode (computed for a Hamamatsu S1223 PIN photodiode with an aperture area of 6.6 mm^2), N_e is the electron flux density through the photodiode, providing an electron-hole current of 0.1 nA, comparable to the dark current of the photodiode; F_e is the total flux of electrons through the photodiode; P_e – electron-hole flux through the photodiode (equal to the value of F_e multiplied by the conversion coefficient of electron-hole pairs at the barrier (F_e-holes coefficient from Table 2); *I_detect* is the resolution value of the current density of the incident electrons in the region of the photodiode.

In computations, the photodiode is modeled as a square with a side of 2.57 mm (the effective area of the photodiode is 6.6 mm^2). Because the flow of particles passing through the aluminum barrier falls on the photodiode surface at an angle, the effective area of the photodiode S_eff decreases (factor $\cos\theta$), which, to a certain extent, compensates for the increase in the number of particles generated in the barrier when an incoming particle falls at large angles to the normal of the vacuum chamber surface. The third column of the table shows the electron beam flux density (n_e/s/cm^2), the fourth column shows the number of incoming electrons that fall into the photodiode aperture, and the fifth column shows the number of these electrons multiplied by the multiplication factor of electron-hole pairs from one electron (last column in Table 2). This amount is converted into photodiode current. The values in the column n_e/s/cm^2 are selected so that the resulting current is equal to the dark current of the photodiode 0.1 nA. The obtained value of the density of beam electron flux is interpreted as the resolution of the photodiode. As can be seen, it is practically independent of the angle of entry of the beam electrons into the vacuum chamber and is ≈0.1 pA/cm^2.

4. ELECTRONIC CIRCUIT

The electron beam in the AREAL accelerator consists of very short electron bunches (less than one ps). The passage of these electrons through the walls of the chamber generates pulses of secondary electrons/positrons/photons with a slightly longer duration. However, from the point of view of measuring electron losses, only the average values of the fluxes are significant; that is, the measuring system must have an integrating property. The measuring system consisted of two boards: a board for pre-integration and amplification and a board for additional amplification, digitization, and data storage. To amplify the weak electrical signals, the operational amplifiers in current or voltage feedback mode are used. When working with photodiodes, especially to provide high speeds, a current feedback circuit is generally used [27] (such amplifiers are called transimpedance amplifiers). The differences and similarities between operational amplifierы based on feedback by voltage and currents are discussed in [28]. In our experiment, BPW34 PIN photodiodes (PHD Sensor) were connected to pre-amplification boards, after which the integrated signals were fed to the board via four channels of 4 × RAM SPI PhW. Here, the signal was additionally amplified using an INA 128 operational amplifier, digitized using the MCP3301 ADC, and parallel recording of the received information into memory microchips (LC512 with a memory capacity of 512 kbit). The 12-bit ADCs used produced a signed output signal within (–4096, 4096). The information was sent through the USB port to the PC using the A_Line_Adapter. A DC source provided power to the 4 × RAM SPI PhW circuit. The board is provided for connecting four photodiodes.

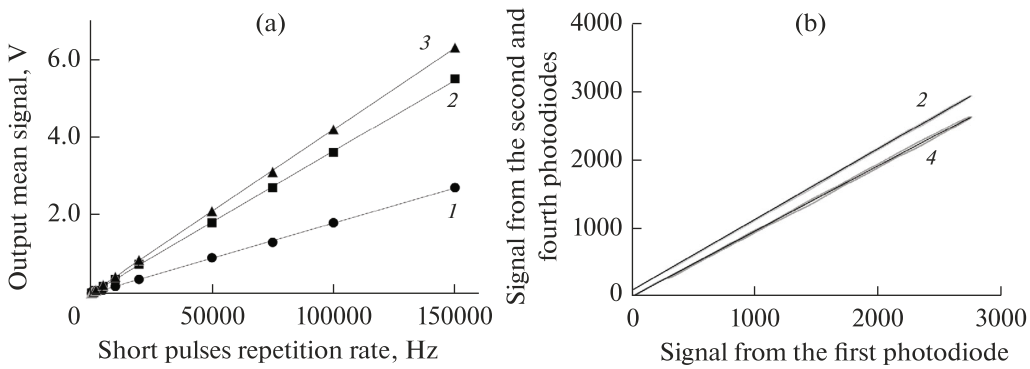

Fig. 3. (a) Signals from primary integrating boards *1, 2, 3.* (b) Comparison of the characteristics of the measuring circuit of photodiodes 2 and *4* with respect to the first photodiode.

5. EXPERIMENTAL PART

5.1. Preliminary Experiments

The purpose of the preliminary experiments was to study the property of integration of the primary amplifier, as well as to compare the characteristics of the channels of the measurement circuit.

Three PIN photodiodes with three primary integrating amplifiers and a fast 4-channel 4×RAM SPI PhW board were used in the experiment. All channels were measured in parallel, which also made it possible to measure the fast signals.

Two preliminary experiments were carried out under the following conditions:

- In the first case, the photodiodes were placed in a black box and coupled to fast LEDs, to which short electrical pulses with a duration of ≈40 ns were applied. The pulse repetition rate was controlled by a frequency generator. Figure 3a shows the results of measurements from the outputs of three integrating boards. The photodiodes were illuminated by LEDs powered by short pulses with different repetition rates.

- In the second one, the characteristics of three integrating channels were compared. To do this, all three photodiodes were illuminated by a single remote light source with adjustable intensity. Figure 3b shows the results of the experiment.

As can be seen from Fig. 3a, the average value of the output voltage is directly proportional to the frequency of the light pulses of the LEDs, that is, the integration is indeed performed. Because of the difference in the parameters of the measuring channels, LEDs, operational amplifiers, and other elements used, the sensitivities of the three manufactured integrating channels differ: for *1*—1.795×10^{-5} V/Hz, *2*—3.645×10^{-5} V/Hz and *3*—4.193×10^{-5} V/Hz. Channel sensitivities concerning light fluxes coincide with an accuracy of +/–5% (see Fig. 3b).

5.2. AREAL Electron Beam Experiments

Experiments at the AREAL electron accelerator were carried out with the power supply of the high-frequency (HF) system of the accelerator turned on/off, with the laser radiation incident on the cathode of the accelerator turned on/off, and also at various beam energies.

Figure 4 schematically shows the beam current, the dark current of the accelerator AREAL, and the location of photodiodes. Because the dark current is formed as a result of the acceleration of random electrons with the RF system turned on and the laser radiation at the cathode turned off, in addition to the broader energy distribution, it should be expected that the angular distribution of electrons is also broader than the angular distribution of beam electrons.

The Background of Light

It is appropriate to mention that in addition to the beam electrons, the photodiodes also recorded light irradiation. Even when the accelerator tunnel was turned off, some light sources were present: the computer screens and illuminated instrument displays. The photodiodes were first placed in a black box, and measurements were taken to evaluate the contributions of these backgrounds. It was found that under such

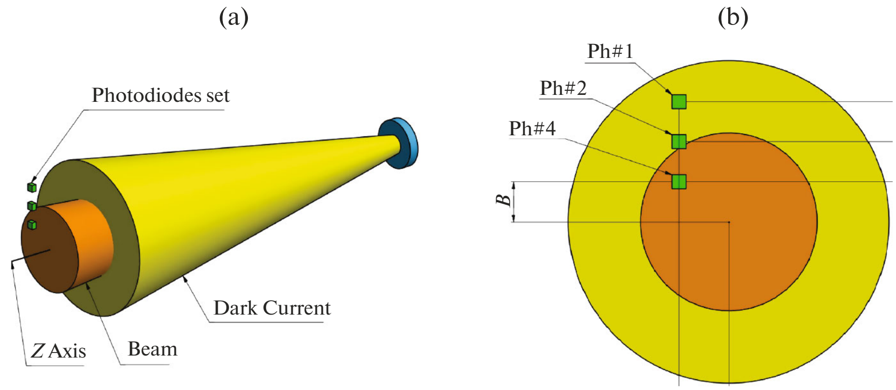

Fig. 4. Isometric view: beam current and dark current. (a) Location of photodiodes in the plane orthogonal to the Z axis of the accelerator, and (b) A and B are the distances of photodiode *4* (lower) from the accelerator axis (horizontally and vertically), W is the distance between photodiodes.

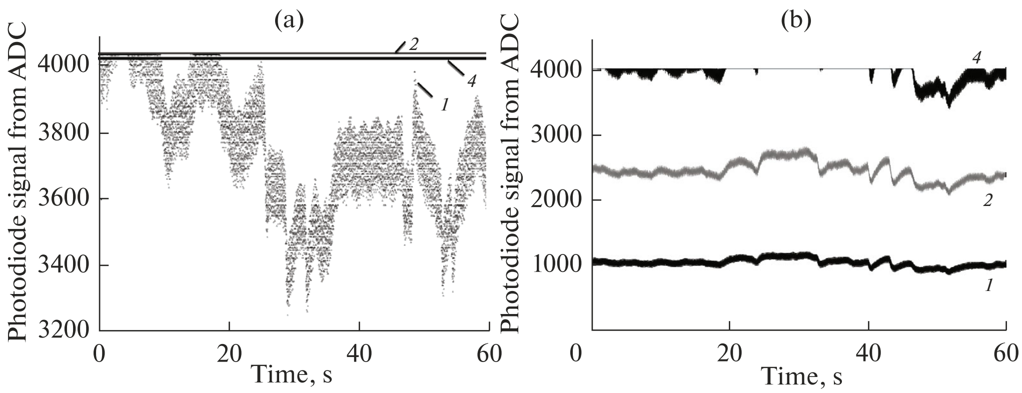

Fig. 5. (a) Readings of photodiodes *1*, *2* and *4* in the plane $Z = 400$ mm, $A = 70$ mm, $B = 0$ mm. (b) Readings of photodiodes *1*, *2* and *4* in the plane $Z = 400$ mm, $A = 70$ mm, $B = 60$ mm.

conditions, the measuring circuit generates a small negative signal, which must be subtracted in subsequent measurements.

Next, an experiment was carried out, where the photodiodes were placed on a tripod in the beam area; the RF system, irradiation of the photocathode with laser radiation, and lighting in the tunnel were turned off. Average values of light background by channels: *1*—7.47; *2*—6.27; *4*—7.46. The values shown are well below the upper limit of 4096 for the MCP3301 12-bit ADC.

Next, two experiments were carried out under the following conditions:

Position $Z = 400$ mm, energy 3.6 MeV ($A \approx 70$ mm, $B \approx 0$ mm, $W = 30$ mm)

The RF system is on, and the photocathode illumination is off (dark current, no beam). Signals were found on all photodiodes (see Fig. 5a). Photodiodes 2 and 4 register an overshoot of the measurement range. The most off-axis photodiode one produces a strong signal near the upper saturation limit. Distances from the beam axis to photodiodes: *1*—138.9 mm; *2*—114.0 mm; *4*—92.2 m.

Position $Z = 400$ mm, energy 3.6 MeV ($A \approx 70$ mm, $B \approx 60$ mm, $W = 30$ mm)

In this experiment, the system of photodiodes was shifted in the direction of increasing the distance from the accelerator axis, so photodiode 4 took the position of the first one in the previous experiment. Distances from the beam axis to photodiodes: *1*—92.2 mm; *2*—76.2 mm; *4*—70.0 mm. In this experiment, the RF system was turned on, and the photocathode illumination was turned off in intervals of 0–20 s and 40–60 s (dark current). In the interval of 20–40 s, the photocathode illumination was switched on, and the dark current and the main beam were present.

The experiment results are presented in Fig. 5b. As can be seen, the readings of all photodiodes began to fall into the measurement range.

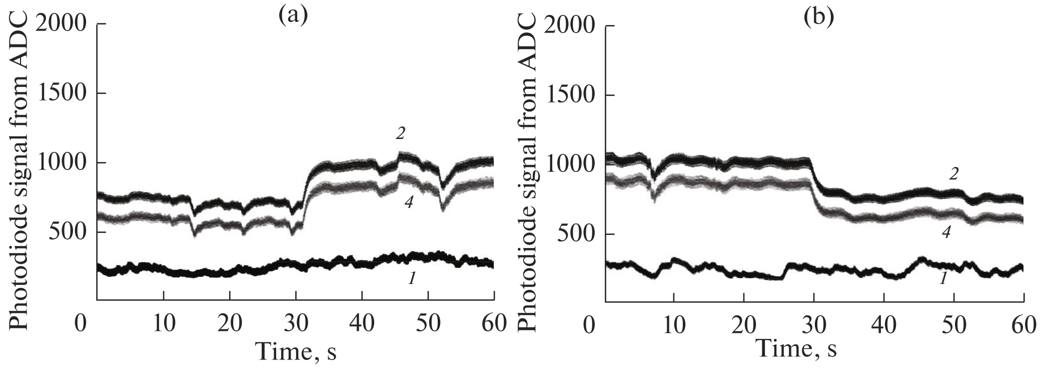

Fig. 6. (a) System of photodiodes *1*, *2*, and 4 on the plane $Z = 1400$ mm. Until the 30th second, only the dark current is present, later - both the dark current and the ground beam. (b) System of photodiodes *1*, *2*, and *4* on the plane $Z = 1400$ mm. Up to the 30th second, there is a dark current and the ground beam, after—only the dark current.

Figure 5b shows the procedure for turning on/off the illumination of the photodiodes, which forms the electron beam. The dark current and the main beam have different transverse dimensions depending on the distance along the Z-axis (see Fig. 4). When the photodiodes are far away from the output flange of the accelerator and are located in the peripheral region of the beam (in the transverse direction) then the beam is no longer felt here, and the dark current is still present. This explains why the switching on the beam is seen rather weakly in Fig. 5b. Placing the photodiodes closer to the beam axis results in the fact that the output signals are saturated (go beyond the allowable measurement limits). Taking this into account, in the next experiment, the photodiodes were brought closer to the beam axis, and the distance from the output flange was increased.

Position $Z = 1400$ mm, energy 3.6 MeV ($A \approx 0$ mm, $B \approx 0$ mm, $W = 30$ mm)

To highlight the transition from the dark current to the beam current, the photodiode system was brought close to the beam axis and moved away along the Z-axis from the output flange. The beam energy is kept at the level of 3.6 MeV. Until the 30th second, only the dark current was present; from the 30th second, the beam current was also switched on. The results of the experiment are shown in Fig. 6a.

As seen in Fig. 6a, the maximum signal was observed for photodiode 2. It follows that the beam axis passed between photodiodes *2* and *4*; the beam was turned on, and this was visible for these two photodiodes, in contrast to the most distant photodiode *1*. The experiment was also carried out in reverse order. The process began with the switched-on beam current, which was switched off on the 30th s. Before the 30th s, both the main beam and the dark current were present; after the 30th s, only the dark current was present. The results of the experiment are shown in Fig. 6b.

It can be seen that in Figs. 6a and 6b, the readings of photodiodes *4* and *2* correlate well with each other and register the beam on/off process.

Position $Z = 1000$ mm, energy 2 MeV ($A \approx 0$ mm, $B \approx 0$ mm, $W = 30$ mm)

The next stage was carried out at a beam energy of 2 MeV; the photodiodes were located on the $Z = 1000$ mm plane. Figure 7a shows the measurement results. During the first 30 s, only the dark current was present; in the next 30 s, the main beam was also switched on.

At the next stage, the experimental conditions were the same, however, the first 30 s measurements were carried out in the presence of a current, and for the next 30 s, only a dark current was present (Fig. 7b).

As can be seen from Figs. 7a and 7b, at a beam energy of 2 MeV only the main beam was observed in the experiments, the dark current was practically absent.

6. CONCLUSION

A comparison is made of beam loss monitoring systems operating on different principles (the use of optical fibers or PIN photodiodes). Under the conditions of the task, namely, to measure the losses of the electron beam in a narrow spatial range outside the SASE100 undulator chamber, a system based on PIN photodiodes is selected and developed.

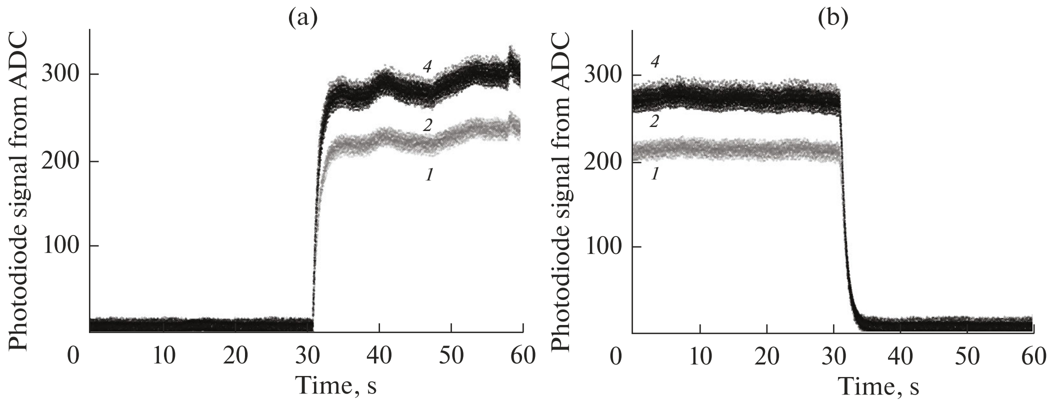

Fig. 7. (a) System of photodiodes *1, 2*, and *4* on the $Z = 1000$ mm plane, turning on the main beam: interval 30–60 s, (b) System of photodiodes *1, 2*, and *4* on the plane $Z = 1000$ mm, switching on the main beam: interval 0–30 s.

The sensitivity of BPW34 and Hamamatsu S1223 photodiodes to an electron beam was estimated and it was concluded that such photodiodes are capable of detecting an electron current in the fA range. A preliminary preamplifier was developed and manufactured, which makes it possible to register short pulses (the duration of electron bunches is in the picosecond range). Adapter cards were tested with short pulses emitted by LEDs. A special system for integrating short light pulses (pulse duration ≈ 40 ns) has been developed and manufactured).

Preliminary experiments at the AREAL accelerator showed that the measurement system indeed integrates short light pulses, as well as pulses of ionizing radiation (primary dark current and accelerated electron beam electrons, as well as possible secondary electrons/positrons and photons).

It was not possible to obtain the absolute characteristics of the electron measurement system in the experiments, because the measurement range of the available Faraday cup does not coincide with our system. The resolution of the Faraday cup was in the range of electron fluxes that saturate PIN photodiodes, that is, the registration system developed by us turned out to be more sensitive.

ACKNOWLEDGMENTS

The authors are grateful to B.A. Grigoryan for posing the problem and for great attention to the work, as well as to the staff of the AREAL accelerator for their help in carrying out the experiments.

FUNDING

The Science Committee of the Republic of Armenia, within the framework of Scientific Projects 20APP-2 G 001 and 21T-2 G 079 financially supported the study.

REFERENCES

1. Tsakanov, V.M., Amatuni, G.A., et al., *NIM A*, 2016, vol. 829, p. 284.
2. Gumprecht, L., Eidam, J., et al., *Status of the Undulator System for the VUV–FEL Phase II*. Annual Report, Desy, Hamburg, 2003, p. 11076.
3. Henschel, H., Korfer, M., Kuhnhenn, J., Weinand, U., and Wulf, F., *NIM A*, 2004, vol. 526, p. 537.
4. Wittenburg, K., *Proceedings of the 2018 CERN–Accelerator–School course on Beam Instrumentation*, (Tuusula, Finland, 2018), pp. 397–435.
5. Wittenburg, K., *AIP CP*, 2000, vol. 546, p. 3.
6. Wittenburg, K., *DESY, Beam Loss Monitors, CAS Beam Instrumentation*, (Hamburg, Germany, 2018), pp. 35,36.
7. Bialowons. W., Ridoutt, F., and Wittenburg, K., *Electron Beam Loss Monitors for HERA*, EPAC 27, London, 1994. p. 1628.
8. Palni, P., Hoeferkamp, M., Taylor, A., Vora, S., McDuff, H., Gua, Q., and Seidel, S., *NIM A*, 2014, vol. 735, p. 213.
9. Srivastava, S., Henry, R., and Topka, A., *JIES*, 2007, vol. 1, no. 1, p. 47.
10. http://usa.hamamatsu.com/cmpdetectors/X-ray.htm

11. Ban, S., Hirayama, H., Namito, Y., et al. *NST*, 1994, vol. 31(2), p. 163.
12. Espinoza, A., *Development of a Silicon Detector for Dose Imaging and Measurement*, University of Wollongong, 2010.
13. Murata, C., Fernandes, D., Lavínia, N., Caldas, L., Pires, S., and Medeiros, R., *RPC*, 2014, vol. 95, p. 101.
14. Shapiro, S.L. and Dunwoodie, W., *NIM A*, 1989, vol. 275, p. 580.
15. Jiménez, F., *Test Procedure for PIN Diode Radiation Detectors*, ININ, México, MRNI-508, 2008, p. 1.
16. Hoeferkamp, M., Grummer, A., Rajen, I., and Seidel, S., *NIM A*, 2018, vol. 890, p. 108.
17. Matsuoka, K., Ichikawa, A., Kubo, H., et al., *NIM A*, 2010, vol. 624, p. 591.
18. Knyazheva, G., Khlebnikov, S., et al., *NIM B*, 2006, vol. 248, p. 7.
19. Mesquita, C., Filho, T., and Hamada, M., *IEEE TNS*, 2003, vol. 50(4), p. 899.
20. Arutunian, S.G., Badalyan, S.A., Chung, M., Lazareva, E.G., Margaryan, A.V., and Harutyunyan, G.S., *RSI*, 2019, vol. 90, p. 073302.
21. Arutunian, S.G., Margaryan, A.V., Harutyunyan, G.S., Lazareva, E.G., Darpasyan, A.T., Gyulamiryan, D.S., Chung, M., and Kwak, D., *RSI*, 2021, vol. 92, p. 033303.
22. Lazareva, E.G., *J. Contemp. Phys.*, 2018, vol. 53(2), p. 136.
23. Tanabashi, M., et al., *Phys. Rev. D*, 2018, vol. 98, p. 030001.
24. Khachatryan, V., *Beam–Matter Interaction and Radiation Dose Measurements*, Armenia, Candle SRI Yerevan, 2019.
25. Bespalov, V.I., *Computer laboratory KL PCLab*, Tomsk: Ed. TPU, 2018 [in Russian].
26. Bespalov V.I., *Lectures on Radiation Protection*, Tomsk: TPU Publishing House, 2017 [in Russian].
27. https://www.scribd.com/document/169316125/si-pd-circuit-e.
28. Karki, J., *Voltage Feedback Vs Current Feedback Op Amps Application Report*, TI SLVA051, 1998.

Translated by V. Musakhanyan